ELSEVIER

Journal of Electroanalytical Chemistry 509 (2001) 31–41

Journal of Electroanalytical Chemistry

www.elsevier.com/locate/jelechem

Electrochemistry of Langmuir–Blodgett and self-organized monolayers of an azocrown ether, both pure and mixed with a phospholipid

Izabella Zawisza [a], Renata Bilewicz [a], Maria Rosa Moncelli [b], Rolando Guidelli [b,*]

[a] *Department of Chemistry, University of Warsaw, Pasteur 1, 02093 Warsaw, Poland*
[b] *Department of Chemistry, University of Florence, Via Gino Capponi 9, 50121 Florence, Italy*

Received 28 September 2000; received in revised form 6 January 2001; accepted 6 January 2001

Abstract

The electrochemical behavior of monolayers of an azocrown ether (L16), both pure and mixed with dioleoylphosphatidylcholine (DOPC) was investigated using a mercury electrode. The monolayers formed at the air | water interface were transferred onto the electrode using the Langmuir–Blodgett approach. The reversibility of the electrode processes depends on the surface pressure during the transfer of the monolayer. The reduction mechanism of the azo to the hydrazo group was studied in acidic medium by cyclic voltammetry and potential-step chronocoulometry. The dependence of the faradaic charge due to azo group reduction at constant pH upon scan rate (for voltammetry) or upon electrolysis time (for chronocoulometry) was examined on the basis of a general kinetic approach. The same approach was used to interpret the dependence of the faradaic charge upon pH at constant scan rate or electrolysis time. The reduction of the azo to the hydrazo group takes place via the reversible uptake of one electron, followed by the rate determining protonation of the resulting radical anion. When L16 is in the form of a pure monolayer its electroreduction is accompanied by a 2D phase transition involving the passage from a liquid-like to a solid-like structure. No such phase transition is observed in mixed L16–DOPC monolayers. At intermediate compositions of this mixture, strong attractive interactions between L16 and DOPC molecules decrease the mean area per molecule with respect to the ideal behavior at the air | water interface, and prevent complete electroreduction of the L16 molecules in the monolayer.

Keywords: Self organized monolayers; Azocrown ether; Langmuir–Blodgett films; Chronocoulometry; Cyclic voltammetry; Kinetics

1. Introduction

Lipophilic or amphiphilic electroactive molecules which are sparingly soluble in water can be readily adsorbed on mercury to form a pure submonolayer or monolayer. Alternatively, the monolayer can be preformed at the air | water interface and transferred onto the mercury surface using the Langmuir–Blodgett (L–B) approach [1,2]. L–B transfers have often been carried out on solid metals such as gold [3,4]. The electroactive molecules can be self-assembled in single-component monolayers or mixed with another compound acting as a diluent of the electroactive sites, e.g. a phospholipid or an alkanethiol [5–9].

Alkanethiols are not ideal diluents for electroactive amphiphilic molecules, due to the lack of flexibility. More flexible, liquid-crystalline monolayers are expected to be better hosts, since they should not hinder any reorientations or conformational changes of the electroactive groups in compact monolayers. Phospholipids may be useful in terms of such flexibility, since they form flexible monolayers at the air | water interface [10,11]. Mixed monolayers of phospholipids with other compounds have been extensively studied at the air | water interface [11–13]. Dioleoylphosphatidylcholine (DOPC) was reported to form a self-organized, liquid-crystalline monolayer of high stability on mercury [14]. Here, the term 'self-organization' will be used to denote the spontaneous organization of adsorbate

* Corresponding author. Tel.: +39-55-2757540; fax: +39-55-244102.
E-mail address: guidelli@unifi.it (R. Guidelli).

0022-0728/01/$ - see front matter
PII: S0022-0728(01)00380-1

molecules into an ordered monolayer at the hanging mercury drop electrode by immersion of the electrode in an aqueous electrolyte with a disordered multilayer spread on its surface, in the absence of any control of its surface pressure. Quinone derivatives, e.g. vitamin K [15], ubiquinone-10 (UQ) [16–18], and viologen [9] were incorporated into phospholipid monolayers supported on mercury and the mechanism of their reduction in the phospholipid monolayer was investigated.

The present work deals with the reduction mechanism of an azocrown ether in monolayers and with the effect of diluting its electroactive molecules with DOPC. Azocompounds are interesting molecules due to their electrochemical and photochemical activity. They exist in two isomeric forms, *Z* (*cis*) and *E* (*trans*) [19,20]. Laviron and Mugnier [21] studied the electrochemical behavior of azobenzene adsorbed on a mercury electrode. The reduction process was found to be pH dependent.

The azobenzene moiety was introduced into the crown ether ring by Shiga et al. [22,23] and Biernat et al. [24,25]. Incorporation of the azo group into a macrocylic ring yields a particularly interesting supramolecular system. It possesses complexing abilities towards metal cations and is both electro- and photoactive [26–30]. Hence its complexation and isomerization processes may be monitored by spectroscopy [27,31] or electrochemistry [28–30].

The two different environments existing in pure and mixed monolayers of electroactive lipophilic molecules may induce some differences in their electrochemical behavior. Thus, a diheptylviologen monolayer adsorbed on mercury from aqueous 0.1 M KBr yields a sharp voltammetric reduction peak and a corresponding reoxidation peak which satisfy the requirements for a process involving a one-electron reduction to the cation radical, accompanied by a 2D phase transition [5]. In a mixed monolayer with DOPC, diheptylviologen is electroreduced in two consecutive steps to the monocationic dimer and the zerovalent monomer, respectively; however, no 2D phase transition is observed [8]. An identical electroreduction mechanism is exhibited by dioctadecylviologen incorporated in a self-organized DOPC monolayer at concentrations ≤ 3 mol% [9]. In this case, however, an inflection in the chronocoulometric charge vs. time curves (Fig. 1 of Ref. [9]) is suggestive of a 2D phase transition not pointed out by the authors. UQ adsorbed on mercury as a pure submonolayer or monolayer yields different cyclic voltammetric peaks corresponding to its reduction to ubiquinol-10, UQH_2, and to reorientation processes within the monolayer [32]. On the other hand, when UQ is incorporated in a self-organized DOPC monolayer [16,17], it yields chronocoulometric charge vs. potential curves whose height increases proportionally to the UQ concentration in the lipid film up to 1 mol%, but then tends to approach a limiting value with a further increase in UQ concentration. This is due to an increasing fraction of UQ molecules segregating within the DOPC monolayer. Evidently, the lack of intercalation of the UQ molecules in the lipid monolayer prevents their electroreduction. It was therefore of interest to investigate the electrochemical behavior of an azocrown ether not only in pure monolayers supported on mercury, but also in mixed monolayers with DOPC.

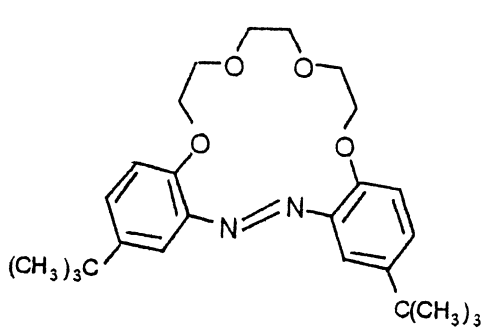

Scheme 1.

2. Experimental

DOPC was purchased from Lipid Products (Surrey, UK). Azocrown L16 (Scheme 1) was synthesized by Biernat et al. [25]. Solutions of DOPC and of azocrown L16 in pentane were prepared daily. The concentration of azocrown L16 in pentane was 1.273×10^{-6} mol ml^{-1}. The distilled water used as the subphase was passed through a Milli-Q water purification system .

The curves of the surface pressure against the molecular area were recorded using the KSV LB trough 5000 equipped with two hydrophobic barriers; a Wilhelmy balance was used as a surface-pressure sensor. Experiments were controlled with a software version KSV-5000. To protect the experimental setup from dust it was placed in a laminar flow hood whose temperature was kept constant at 20 ± 1°C. Surface potential and surface pressure were recorded simultaneously as a function of the molecular area. The limits of the experimental accuracy were ~ 0.2 nm^2 molecule^{-1} for the molecular area, and ~ 1 mN m^{-1} for the surface pressure. L–B monolayers were transferred onto a thin mercury film electrode (TMFE) at different surface pressures by immersing the electrode at a speed of 4 mm min^{-1}. The TMFE was obtained from a silver wire precleaned in concentrated perchloric acid; this was touched to a mercury drop and cathodically polarized in 0.1 M KOH to obtain a shining and uniform layer of mercury, ca. 1 μm thick. The surface area of the TMFE was typically 0.5 cm^2, but disk electrodes of larger area were also employed for a more accurate estimate of the transfer ratio. This ratio, defined as the ratio of the decrease in surface area of the monolayer on water to

the surface area of the electrode onto which the monolayer is transferred, was measured under software control. Transfer ratios were close to 1, pointing to quantitative transfer onto the electrode.

Electrochemical measurements were carried out with a potentiostatic three-electrode system, using either the TMFE or a home-made hanging mercury drop electrode (area 1.41×10^{-2} cm^2) as a working electrode, a platinum foil as an auxiliary electrode, and a 1 M NaCl calomel electrode as a reference electrode. All potentials are referred to this electrode. The hanging mercury drop electrode and the cell are described in detail elsewhere [33]. All measurements were carried out in aqueous 0.1 M $NaClO_4$. The pH range from 2.5 to 3 was controlled with $HClO_4$, that from 3 to 6 with mixtures of 1.5×10^{-2} M citric acid and NaOH. The electrolytic solution was deaerated by purging with high purity argon for not less than 20 min. After deaerating, amounts of azocrown L16 or of DOPC–azocrown L16 mixtures in pentane, corresponding to about three monolayers, were spread on the surface of the electrolytic solution. After allowing the pentane to evaporate, the mercury electrode was immersed in the electrolytic solution across the insoluble film. During such an immersion a monolayer of azocrown L16 or of a DOPC–azocrown L16 mixture self-organizes on the mercury surface. Distinct from BLMs [34] mixed monolayers deposited on mercury cannot have a composition different from that of the membrane-forming mixture. In fact, the time τ during which the mercury drop remains in contact with the film spread on the surface of the aqueous electrolyte is of the order of 2 s. Let us assume as a limiting case that L16 tends to be completely expelled from the L16–DOPC mixture in contact with mercury: the quantity of L16 that may actually escape from the drop surface must be necessarily less than that diffusing across the maximum contact line among mercury, solution and argon (namely $2\pi r$, where $r \sim 0.035$ cm is the drop radius) during τ under limiting conditions, namely for a zero surface concentration of L16 along this line. This quantity is given by $(2\pi r)2xN(D\tau/\pi)^{1/2}$, where x is the mole fraction of L16 in the L16–DOPC mixture, N is the mole number per unit surface of all the species composing the monolayer, D is the diffusion coefficient of L16, and $(\pi Dt)^{1/2}$ is the diffusion layer thickness at a given time $t \leq \tau$. For the typical values $r = 0.035$ cm, $D = 2 \times 10^{-8}$ cm^2 s^{-1}, $N = 2 \times 10^{-10}$ mol cm^{-2}, and $x = 0.15$, this quantity equals 1.49×10^{-15} mol and, hence, is only 0.32% of the quantity of L16 dragged into the solution by the mercury drop.

The properties of the monolayers so obtained were studied by a.c. voltammetry, cyclic voltammetry and chronocoulometry, using an Autolab instrument (Echo Chemie) supplied with a FRA2 module for impedance measurements, SCAN-GEN scan generator and GPES3 software. Chronocoulometric measurements were also carried out with a wholly computerized apparatus [35] following a procedure described elsewhere [36]; the microprocessor used to control all operations was a Model NOVA 4X from Data General (Westboro, MA), whereas an Amel Model 551 (Milano, Italy) fast-rise potentiostat was employed for the potentiostatic control of the three-electrode system. Each chronocoulomogram consisted of a series of consecutive potential jumps of progressively increasing height from a fixed initial value $E_i = 0.0$ V to different final values E ranging from E_i to -0.400 V; E was shifted progressively toward more negative values by -10 mV increments. Each chronocoulomogram was recorded on a single monolayer-covered mercury drop. The charge $Q(t,E)$ following each potential jump $E_i \rightarrow E$ was recorded vs. the time t elapsed from the instant of the jump for 100 ms, after which the potential was stepped back to E_i where it remained for 10 s. During this period the reduction product of L16 is completely reconverted to the reactant, provided E is not so negative as to cause the irreversible opening of the ring (see further). Thus, an increase in the rest time at E_i beyond 10 s leaves the charge $Q(t,E)$ practically unaltered.

3. Results and discussion

3.1. L–B transfer of azocrown ether onto the TMFE

Monolayers of azocrown L16 were transferred from the air | water interface onto the electrode surface at different surface pressures, and hence at different areas per molecule. Fig. 1 shows the cyclic voltammograms recorded after L–B transfers at 5, 22, 27 and 30 mN m^{-1}. More reversible voltammograms (smaller peak-to-peak separation) are obtained at lower surface pressures, when the interactions between the molecules are weaker. The number of electroactive molecules, as estimated from the charge under the negative peak for a two-electron reduction, agrees with the total number of molecules transferred from the air | water interface only when the transfer is performed close to the collapse pressure. Under high surface-pressure conditions, the lower reversibility and the presence of a discontinuity in the voltammogram are suggestive of the occurrence of a 2D phase transition in the L16 monolayer following its electroreduction (see further for a tentative interpretation). Above the collapse pressure ($\Pi = 30$ mN m^{-1}), the anodic signal is very poorly developed and the charge under the negative peak exceeds that, 28.6 μC cm^{-2}, estimated for the reduction of one full monolayer (for such an estimate see further, Section 3.3). This can be attributed to the formation of aggregates and crystallization processes [37]. Only at very low scan rates (≤ 5 mV s^{-1}) can the positive peak be resolved from the current due to mercury oxidation.

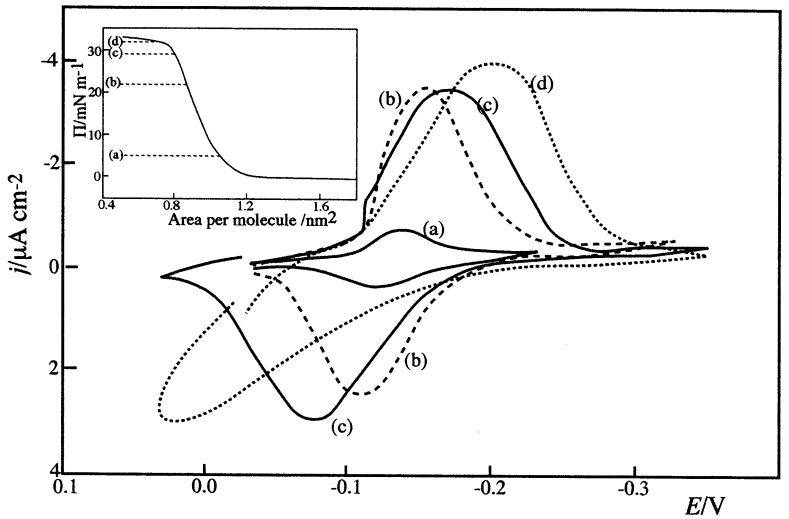

Fig. 1. Cyclic voltammograms obtained by L–B transfer of a L16 monolayer from the air | water interface onto the TMFE at different surface pressures: (a) 5; (b) 22; (c) 27; and (d) 30 mN m^{-1} in 0.1 M $NaClO_4$; pH 4.1; $v = 0.01$ V s^{-1}. The inset shows the curve of the surface pressure against the area per molecule of L16 at the air | water interface. The dashed lines mark the pressures adopted for the L–B transfer.

In order to find the equilibrium spreading pressure the following experiment was performed. A sample of the compound corresponding to 2–3 monolayers was deposited on the water surface and left until the surface pressure attained a constant value. The equilibrium surface pressure was estimated at 25.3 mN m^{-1}. Under these conditions the monolayer was transferred onto the TMFE and the charge obtained was 28 ± 2 μC cm^{-2}, which corresponds to full electroreduction of a monolayer. Further experiments were performed under conditions of equilibrium spreading pressure. The monolayer transferred onto the TMFE by this procedure exhibits the same electrochemical properties as those of the monolayer self-organized on the hanging mercury drop electrode, including the differential capacitance after electroreductive cleavage of the azocrown ether L16 to the amine.

3.2. Pure azocrown L16 monolayer at the mercury | solution interface

Three consecutive cyclic voltammograms and the curves of the quadrature component of the electrode admittance against the applied potential for a pure L16 monolayer on a mercury electrode are shown in Fig. 2. The first cyclic voltammogram (curve a in Fig. 2A) covers the potential range from -0.1 to -0.36 V and shows a reduction peak (peak I_{red}) and the corresponding oxidation peak (peak I_{ox}). They are due to the electroreduction of the azo to the hydrazo group, which consumes two electrons and two protons according to the overall reaction [38]:

$$-N=N- \; + 2e^- + 2H^+ \Leftrightarrow \; -NH-NH- \qquad (1)$$

and to the reverse electrode reaction. The second cyclic voltammogram (curve b) covers the potential range from -0.1 and -1.0 V and shows two reduction peaks; the first is due to the electrode reaction (1), while the second (peak II_{red}) corresponds to the further reduc-

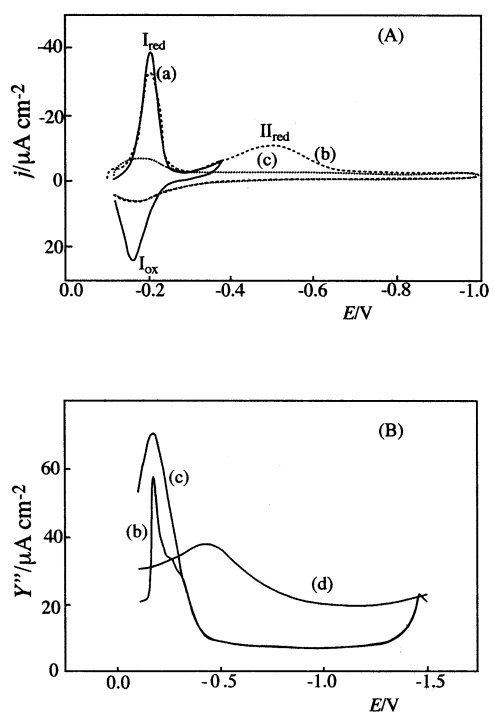

Fig. 2. (A) Three consecutive cyclic voltammograms of a L16 self-organized monolayer on mercury from a pH 4.1 aqueous solution of 0.1 M $NaClO_4$ at a scan rate $v = 0.1$ V s^{-1}; (a) scan from -0.1 to -0.36 V; (b) scan from -0.1 to -1.0 V; and (c) repeated scan from -0.1 to -1.0 V. (B) Y'' vs. E curves of a pH 4.1 aqueous solution of 0.1 M $NaClO_4$ on bare mercury and (d) on mercury coated with a L16 monolayer (b: first scan; c: second scan).

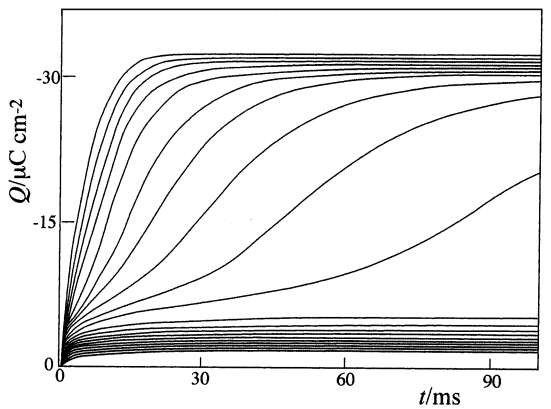

Fig. 3. Charge vs. time curves for a L16 monolayer on mercury in a pH 4.5 aqueous solution of 0.1 M $NaClO_4$, obtained by jumping from $E_i = 0.0$ V to different final potentials E. From bottom to top, the curves refer to E values varying from -0.100 to -0.300 V by -10 mV increments.

tion of the hydrazo group to the amine, which also consumes two protons and two electrons:

$$-NH-NH- \; + 2e^- \; + 2H^+ \; \rightarrow \; -NH_2\,{}_2HN- \qquad (2)$$

The latter electrode reaction causes the breaking of the hydrazo bond and the resulting opening of the ring. Such an opening is irreversible, which explains the lack of reoxidation peaks in the reverse potential scan. The subsequent cyclic voltammogram (curve c) shows neither reduction nor oxidation peaks, because the previously formed amine is electroinactive.

Even after amine formation with ring opening, the product remains on the electrode surface, as indicated by the fact that the curve of the quadrature component, Y'', vs. the applied potential E, does not change in the consecutive scans on the same azocrown-coated mercury drop over the potential range from -0.4 to -1.5 V (see Fig. 2B). Y'' maintains an almost constant value of 6.80 μF cm^{-2} over the potential range from -0.50 to -1.20 V. In the first negative potential scan of Y'' (curve b in Fig. 2B), a peak is observed over the potential range of the first voltammetric peak I_{red} of Fig. 2A; this may be partly ascribed to an incompletely resistive contribution to the faradaic impedance from the corresponding electrode reaction; conversely, no peak in the Y'' vs. E curve is observed over the potential range of the more negative voltammetric peak in Fig. 2A. In the second negative potential scan (curve c in Fig. 2B) carried out after the rupture of the –HN–NH– bond, a peak in the Y'' vs. E curve is still observed at approximately the same potential of -0.18 V, albeit of different shape. Since in this case no faradaic process can be invoked, this peak must be ascribed to some reorganization of the amine molecules within the film. This also explains the presence of the two small negative and positive rounded humps in the cyclic voltammetric curve c of Fig. 2A, obtained under the same experimental conditions after L16 electroreduction to the amine.

Fig. 3 shows a series of chronocoulometric curves of the charge Q vs. time t obtained from a pH 4.5 buffered solution by jumping from a fixed initial potential $E_i = 0.0$ V to progressively more negative final potentials E, by -10 mV increments. At the less negative E values, where L16 is still electroinactive, the charge $Q(t)$ increases rapidly in a few milliseconds, due to the charging of the interphase, and then remains constant in time. As E becomes progressively more negative $Q(t)$ increases in time first abruptly, due to the capacitive contribution, and then more slowly, due to the gradual electroreduction of the L16 monolayer. Ultimately, at the most negative potentials, the electroreduction rate becomes so high as to convert the azocrown to the hydrazocrown ether in a few milliseconds, after which the charge becomes time independent. The $Q(t)$ vs. t curves in Fig. 3 show an inflection point: this is typical of electrode processes involving nucleation and growth [39,40]. The presence of an inflection point in potentiostatic charge vs. time curves is equivalent to the presence of a minimum, followed by a maximum and by an exponential decay to zero, in the corresponding potentiostatic current–time curves. This typical behavior is commonly interpreted as a 2D phase transition involving a time-dependent nucleation and growth. It is observed both in a potential-induced transition from a disordered, liquid-like state, of an electroinactive adsorbate to an ordered, solid-like state [41,42] or during an electrochemical reaction [43–47]. In the present case the 2D phase transition is associated with the electroreduction of the azo to the hydrazo group, and is therefore electrochemical in nature. The 2D nucleation of the hydrazo molecules resulting from L16 electroreduction, as well as the growth of the nuclei, can be tentatively explained by the formation of N – H···N hydrogen bonds between adjacent molecules. In other words the critical nuclei and the aggregates resulting from their growth may be regarded as consisting of a network of H-bonded hydrazo molecules, oriented in such a way as to favor such an H-bonding. It is also possible that the 2D condensation may be induced by the appreciable configurational changes that accompany L16 electroreduction to the hydrazo form. In fact, such an electroreduction involves an appreciable increase in the length of the nitrogen–nitrogen bond [48] and a change in the angle between the two aromatic rings.

Fig. 4 shows a series of curves of the charge, Q(100 ms, E), at a constant electrolysis time of 100 ms against E for different pH values. In recording all these curves the initial potential E_i was set equal to 0.0 V. More positive E_i values were avoided to exclude partial disorganization of the L16 film and mercury oxidation. The potential E of these curves at constant faradaic charge

shifts by about 60 mV toward more negative values per each unitary increment of pH. It should be noted that the Q(100 ms, E) vs. E curve at pH 2.5 in Fig. 4 is lower than those at higher pH values, and is also normally less reproducible. This is probably to be ascribed to the formal potential of the azocrown–hydrazocrown ether redox couple approaching more closely to the initial potential E_i adopted in chronocoulometric measurements, as the pH is decreased. Hence, the rate of hydrazocrown ether reoxidation to the azocrown form at the fixed initial potential E_i decreases with decreasing pH, preventing a complete L16 regeneration during the rest time at E_i.

It is interesting to observe that the presence of 1.25×10^{-4} M $HClO_4$ in the absence of the citric buffer is not sufficient to prevent the depletion of hydrogen ions in the immediate vicinity of the L16 monolayer during electrolysis at potentials corresponding to the plateau of the Q(100 ms, E) vs. E curves. At these potentials the L16 monolayer acts as a proton sink consuming two protons per adsorbed molecule as soon as they reach the electrode surface under diffusion limiting conditions. In other words, during the first stages of electrolysis, $Q(t)$ is controlled by the diffusion of protons toward the electrode and increases linearly with $t^{1/2}$, in accordance with the Cottrell equation:

$$Q(t) = Q_{cap} + 2F[H^+]^* \sqrt{(D_{H^+} t/\pi)} \quad (3)$$

Here Q_{cap} is the capacitive charge, and $[H^+]^*$ and $D_{H^+} \sim 10^{-4}$ cm^2 s^{-1} are the bulk concentration and the diffusion coefficient of protons. Once the charge corresponding to complete L16 electroreduction is attained, $Q(t)$ remains constant in time. In fact, the concomitant diffusion of protons toward the electrode, ultimately leading to the annihilation of their diffusion layer thickness, has no effect on the faradaic charge. Fig. 5 shows the experimental $Q(t)$ vs. t curve at $E = -0.250$ V in 1.25×10^{-4}M $HClO_4$ as well as the corresponding $Q(t)$ vs. $t^{1/2}$ plot; the latter is indeed linear with a slope of 4.5 μC cm^{-2} ms$^{-1/2}$ up to the attainment of the maximum limiting charge, in fairly good agreement with the value, 4.3 μC cm^{-2} ms$^{-1/2}$, estimated from the Cottrell equation.

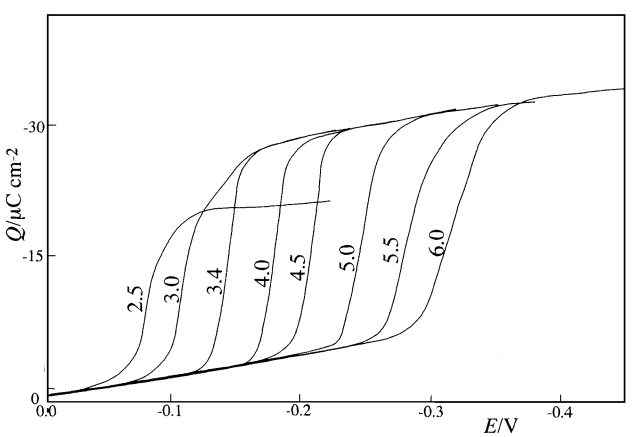

Fig. 4. Q(100 ms, E) vs. E curves for a L16 monolayer on mercury in buffer solutions of 0.1 M $NaClO_4$ at different pH values. Numbers on each curve refer to the pH value.

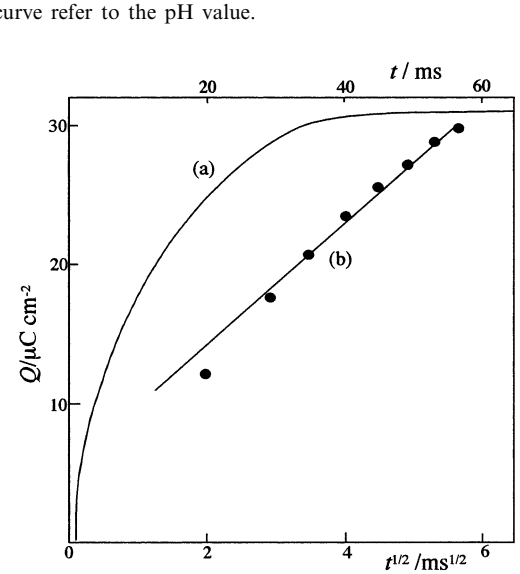

Fig. 5. $Q(t)$ vs. t curve for a L16 monolayer on mercury in 1.25×10^{-4} M $HClO_4$ at: (a) $E = -0.250$ V; and (b) corresponding $Q(t)$ vs. $t^{1/2}$ plot.

3.3. Mixed L16–DOPC monolayers at air | water and mercury | solution interfaces

The azocrown ether L16 was mixed with the electroinactive DOPC and the behavior of the two-component monolayers was studied at the air | water and mercury | solution interfaces. Incidentally, the behavior of a mixed monolayer of octadecanol and 1-pyrenenonanol at the air | solution and Au(111) | solution interfaces was recently investigated by Bizzotto et al. [49]. The mixing properties of the two components at the air | water interface were checked by recording curves of the surface pressure against the molecular area for different L16 to DOPC ratios in the spreading solution. The DOPC monolayer, thanks to the presence of a double bond in the hydrocarbon tail, is in the liquid crystalline state at room temperature, thus providing a flexible matrix, which can easily accommodate the stiff azocrown molecules. In the case of vanishingly small or equal interaction energies between the molecules of the two components of the monolayer (i.e. in the case of ideal behavior), the surface pressure corresponding to the collapse of the film, Π_{coll}, and the limiting area per molecule, A_0, are expected to vary linearly from the value for one pure component to the value for the other with an increase in the mole fraction of the second component [50]:

$$\Pi_{coll} = \Pi_{coll,1} X_1 + \Pi_{coll,2} X_2 \quad (4)$$

$$A_0 = A_{0,1}X_1 + A_{0,2}X_2 \quad (5)$$

Here Π_{coll} is the collapse surface pressure for a mixed monolayer consisting of X_1 and X_2 mole fractions of the two components, whereas $\Pi_{coll,1}$ and $\Pi_{coll,2}$ are the corresponding values for the two pure components. Analogously, A_0, $A_{0,1}$, $A_{0,2}$ are the limiting molecular areas in the mixed monolayer and in the monolayers of the two pure components.

Fig. 6 shows the experimental values of the collapse pressure and of the molecular area as a function of the mole fraction of L16: the molecular area was obtained by extrapolation to zero surface pressure. The collapse pressure varies linearly with the mole fraction of the azocrown ether. This denotes a good miscibility of phospholipid and azocrown molecules for all compositions of the mixture. On the other hand, the area per molecule shows notable deviations from a linear dependence on monolayer composition. Perfectly analogous behavior is obtained by using the molecular area at collapse. Only when the mole fraction of L16 is small does the area per molecule agree with the ideal behavior. When this mole fraction is > 0.4 the mean molecular area calculated from the experimental isotherm is smaller than that corresponding to the ideal linear behavior. This denotes the presence of strong interactions between unlike molecules, which may even give rise to aggregates. Formation of aggregates or micelles in mixed monolayers is indeed responsible for negative deviations of the mean molecular area from the ideal behavior [50].

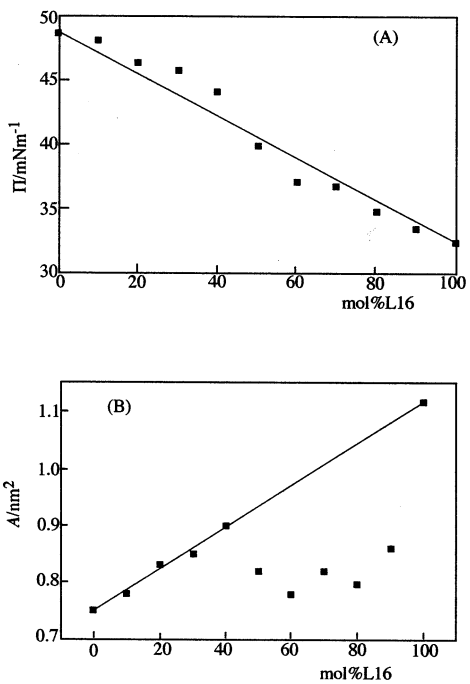

Fig. 6. Collapse pressure (A) and area per molecule (B) of a mixed L16–DOPC monolayer spread on an aqueous subphase as a function of the L16 mole fraction. The solid straight lines express the ideal behavior.

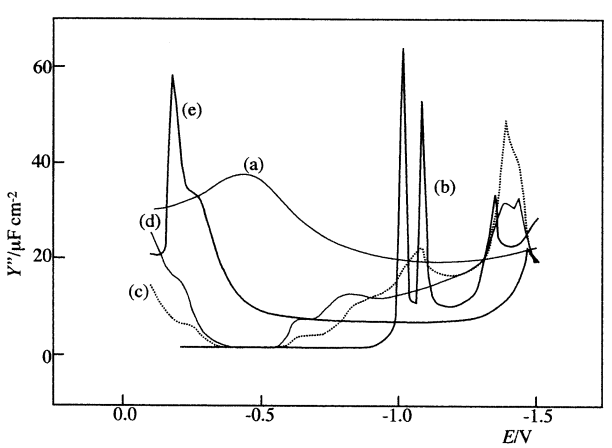

Fig. 7. Y'' vs. E curves for a pH 4.1 aqueous solution of 0.1 M $NaClO_4$ on: (a) bare mercury and on mercury coated with mixed L16–DOPC monolayers containing (b) 0; (c) 20; (d) 50; and (e) 100 mol% L16.

The electrochemical behavior of L16 in mixed L16–DOPC monolayers of different composition was investigated by self-organizing these monolayers on a hanging mercury drop electrode. A self-organized monolayer of pure DOPC turns the polar heads toward the aqueous phase and the hydrocarbon tails toward the hydrophobic mercury surface. Over the potential range from -0.20 to -0.75 V versus SCE this monolayer behaves like a half-membrane [14,51,52]. Thus, it is practically impermeable to inorganic ions and its differential capacitance amounts to 1.7–1.8 μF cm^{-2}, namely it is twice that of solvent-free black lipid membranes. At more negative potentials, the quadrature component of the electrode admittance shows three peaks (see curve b in Fig. 7), which are due to different degrees of reorientation of the lipid molecules. Fig. 7 illustrates the changes in Y'' of mixed L16–DOPC monolayers when passing from pure DOPC to pure L16. An increase of the L16 content in the film narrows the potential range over which Y'' coincides with the differential capacitance of DOPC alone. Naturally, over the potential range in which L16 is electroactive, its reduction current also affects Y'', which can no longer be identified with the differential capacitance. The increase in Y'' observed at potentials positive of -0.25 V is to be ascribed to the electroreduction of the L16 molecules and to their reorganization as well. At potentials negative of -1.0 V, a gradual increase in the L16 content causes the two less negative peaks of DOPC first to merge into a single peak, and ultimately to disappear, while the third, more negative peak shifts toward more negative potentials.

Fig. 8 exemplifies the typical behavior of the chronocoulometric charge vs. time curves of L16–DOPC mixed monolayers observed for L16 mole fractions $< 90\%$. These curves were obtained from a 20 mol%

L16 mixed monolayer in a pH 4.0 buffered solution by jumping from $E_i = 0.0$ V to progressively more negative final potentials E, by -10 mV increments. As distinct from the $Q(t)$ vs. t curves of a pure L16 monolayer, the curves of L16–DOPC mixed monolayers do not show an inflection, thus excluding nucleation and growth of clusters of the hydrazo form during L16 electroreduction. Just as for the case a pure L16 monolayer, the Q(100 ms, E) vs. E curves of mixed L16–DOPC monolayers at different pH values shift by about 60 mV toward more negative values per each unitary increment of pH.

Fig. 9 shows the overall faradaic charge involved in the electroreduction of L16 as a function of its mole fraction in the L16–DOPC monolayer, as estimated from the height of the $Q(t = 100,\ E)$ vs. E curves recorded in pH 4.0 aqueous solutions of 0.1 M $NaClO_4$. The solid curve in the same figure was calculated by allotting to the L16 and DOPC molecules in the mixed monolayer the molecular areas of 1.12 and 0.75 nm^2, as estimated from L–B experiments (see Fig. 6B), and by assuming that all the L16 molecules undergo a two-electron reduction to the hydrazo form. In particular,

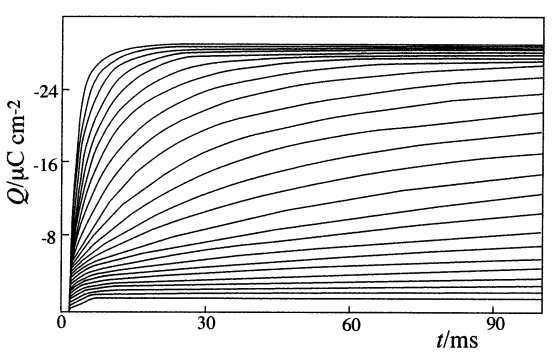

Fig. 8. Charge vs. time curves for a 20 mol% L16 mixed monolayer on mercury in a pH 4.0 aqueous solution of 0.1 M $NaClO_4$, obtained by jumping from $E_i = 0.0$ V to different final potentials E. From bottom to top, the curves refer to E values varying from -0.110 to -0.350 V by -10 mV increments.

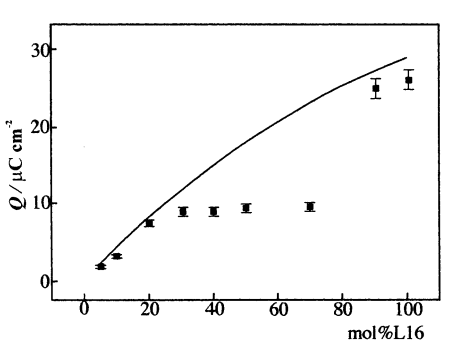

Fig. 9. Overall faradaic charge for L16 electroreduction in mixed L16–DOPC monolayers on mercury from pH 4.0 aqueous solutions of 0.1 M $NaClO_4$, as a function of the L16 mole fraction. The solid curve was calculated as described in the text.

the calculated charge for a pure L16 monolayer amounts to 28.6 $\mu C\,cm^{-2}$. Up to 30 mol% L16, the experimental faradaic charge agrees with the calculated value. At higher L16 mole fractions, the faradaic charge is less than the estimated value and assumes rather irreproducible values ranging from 7 to 9 $\mu C\,cm^{-2}$ until the L16 mole fraction approaches 90%. From 90 to 100 mol% L16, the faradaic charge attains values close to the calculated ones, and the corresponding $Q(t)$ vs. t curves show the inflection typical of a 2D condensation.

At L16 mole fractions less than 30%, the reoxidation of hydrazocrown ether to the azo form occurs in a few tens of milliseconds after the backward potential jump, $E \rightarrow E_i$. This very short time is to be compared with the much longer rest time at E_i, ~ 10 s, which is required for the complete reoxidation of a pure hydrazocrown ether monolayer. This indicates that such a long rest time is to be ascribed to a lower electrooxidation rate of the solid-like form of the pure hydrazo monolayer following 2D condensation. The absence of a 2D condensation in L16–DOPC monolayers is probably due to strong hydrophobic interactions between L16 and DOPC molecules; these should prevail over the interactions between neighboring hydrazo molecules. Over the L16 mole fraction range from 30 to 90% these interactions are so effective as to decrease the average molecular area at the air | water interface (Fig. 6B) and to block an appreciable amount of L16 molecules under some form of aggregation. These blocked L16 molecules are electroinactive, at least in the time scale of chronocoulometric measurements. Thus, the charge following a potential step from $E_i = 0.0$ V to a sufficiently negative value attains its limiting value in a few milliseconds, due to the rapid electroreduction of a well-defined amount of L16 molecules, and then remains constant in time, as appears from Fig. 8. This implies that the remaining fraction of L16 molecules present in the mixed film shows no tendency to be electroreduced during the 100 ms of electrolysis. It should also be noted that when the interactions between L16 and DOPC molecules start to cause a decrease in the overall faradaic charge with respect to the calculated value, the minimum rest time at E_i required to reoxidize the reduced form of the electroactive fraction of L16 molecules increases, attaining values of the order of 3–5 s.

3.4. Electroreduction mechanism of a pure azocrown L16 monolayer on mercury

In cyclic voltammetric measurements, the mechanism of the electrode reaction of Eq. (1) in acidic medium was investigated on the basis of the dependence of peak I_{red} of Fig. 2A upon the scan rate v at constant pH and upon pH at constant v. Over the whole pH range from

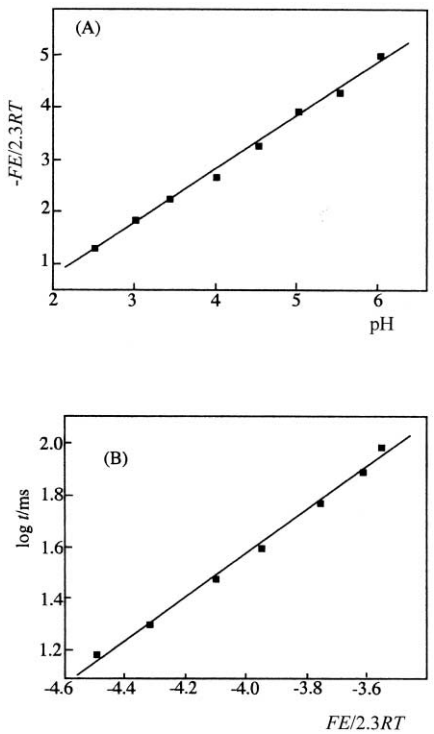

Fig. 10. Plot of $-FE/(2.3RT)$ vs. pH at constant electrolysis time $t = 100$ ms and at constant faradaic charge $Q_f = 10$ μC cm^{-2} (A), and plot of log t vs. $FE/(2.3RT)$ at constant pH 4.5 and at constant faradaic charge $Q_f = 14$ μC cm^{-2} (B), as obtained from chronocoulomograms of a pure L16 monolayer on mercury in aqueous 0.1 M $NaClO_4$.

2.5 to 6.5, peak I_{red} is practically symmetric with respect to the peak potential. Since the charge under peak I_{red} is practically constant with varying scan rate and pH, the peak potential E_p is a potential corresponding to a constant faradaic charge Q_f, and the general approach of Ref. [17] can be employed. This approach holds for an electrode reaction consisting of a series of consecutive elementary steps, only one of which is rate determining. Let the algebraic sum of all elementary steps preceding the rate-determining one be expressed by the general equation:

$$rR + hH^+ + \vec{n}e^- \Leftrightarrow I \tag{6}$$

Here R denotes the reactant, r and h are stoichiometric coefficients, $\vec{n}$ is the number of electrons exchanged before the rate determining step (rds), and I is the intermediate involved in the rds. Let us further ascribe to the rds involving the intermediate I the general form:

$$iI + h'H^+ + \delta e^- \rightarrow \text{products} \tag{7}$$

where i and h' are the molecularities of the rds with respect to the intermediate I and the protons, respectively. The dependence of a potential corresponding to a constant faradaic charge (and hence, in our case, the peak potential E_p) upon the scan rate v at constant pH is given by [17]:

$$\frac{RT}{F}\left(\frac{\partial \ln v}{\partial E_p}\right)_{pH} = -(i\vec{n} + \delta\beta) \tag{8}$$

where β is the symmetry factor for the rds, if it is electrochemical, namely if $\delta \neq 0$. The dependence of E_p upon pH at constant v is given by:

$$\frac{F}{2.3RT}\left(\frac{\partial E_p}{\partial pH}\right)_v = -\frac{ih + h'}{i\vec{n} + \delta\beta} \tag{9}$$

The plot of ln v vs. $FE_p/(RT)$ at constant pH 4.1 is a straight line of slope -0.91, very close to -1. Since the symmetry factor β is expected to assume a value close to 0.5, in view of Eq. (8) such a slope implies that $\delta = 0$ and $i = \vec{n} = 1$, namely that the rds is a chemical step preceded by the electron transfer step in quasi equilibrium yielding the $[–N–N–]^{\bullet -}$ anion radical. The $FE_p/(2.3RT)$ vs. pH plot at constant scan rate $v = 0.1$ V s^{-1} is also a straight line of slope -1.05, very close to -1. In view of Eq. (9) and of the unit value of $(i\vec{n} + \delta\beta)$, two alternative pathways are possible, namely a protonation step preceding the rds ($h = 1$, $h' = 0$) or a protonation rds ($h = 0$, $h' = 1$). Since the rds is chemical ($\delta = 0$), it is realistic to conclude that the rds is a protonation step following the uptake of the first transferring electron. The rds is then followed by the uptake of a further electron and a further proton in quasi equilibrium, yielding the hydrazo compound:

$$R + e \Leftrightarrow R^{-\bullet}; \quad R^{-\bullet} + H^+ \overset{rds}{\rightarrow} RH^{\bullet};$$
$$RH^{\bullet} + e + H^+ \Leftrightarrow RH_2 \tag{10}$$

The height of the sigmoidal chronocoulometric $Q(100\text{ ms}, E)$ vs. E curves in Fig. 4 was estimated from the vertical distance between the plateau and the linear extrapolation of the corresponding foot, so as to correct for the capacitive contribution. The resulting overall faradaic charge amounts to about 26 μC cm^{-2} for the reduction of the L16 monolayer, in fairly good agreement with the cyclic voltammetric value and with the value estimated from LB measurements. At constant faradaic charge $Q_f = 10$ μC cm^{-2} and at constant electrolysis time $t = 100$ ms, the plot of $FE/(2.3RT)$ vs. pH is linear, with a slope equal to -1 (see Fig. 10A). This behavior agrees once again with the mechanism of Eq. (10). In fact, the treatment of the general mechanism of Eqs. (6) and (7), as applied to chronocoulometric measurements, yields the equations [16]:

$$\frac{RT}{F}\left(\frac{\partial \ln t}{\partial E}\right)_{pH,Q} = (i\vec{n} + \delta\beta) \tag{11}$$

and

$$\frac{F}{2.3RT}\left(\frac{\partial E}{\partial pH}\right)_{t,Q} = -\frac{ih + h'}{i\vec{n} + \delta\beta} \tag{12}$$

These equations are analogous to Eqs. (8) and (9) for the voltammetric case, apart from the replacement of the peak potential E_p with a chronocoulometric final

potential E at constant faradaic charge Q_f, and of the scan rate v with the reciprocal of the electrolysis time t. The plot of log t vs. $FE/(2.3RT)$ at pH 4.5 and $Q_f = 14$ μC cm^{-2} in Fig. 10B, as obtained from the chronocoulometric $Q(t)$ vs. t curves, is linear and exhibits a slope equal to unity. Unit values for the quantities $(ih + h')/(i\vec{n} + \delta\beta)$ and $(i\vec{n} + \delta\beta)$ are in agreement with the mechanistic conclusions drawn from the cyclic voltammetric measurements.

4. Conclusions

The electroreduction mechanism of azocrown L16 to the hydrazo form on mercury involves the reversible uptake of one electron, followed by the rate determining protonation of the resulting radical anion. When L16 is in the form of a pure self-organized monolayer, its electroreduction is accompanied by a 2D phase transition involving the passage from a liquid-like to a solid-like structure. The latter structure requires a relatively long time (~ 10 s) for its complete reoxidation at $E_i = 0.0$ V. In mixed L16–DOPC monolayers, the attractive interactions between L16 and DOPC molecules prevail. Thus, a 2D phase transition is observed only at L16 concentrations > 90 mol%. At L16 concentrations < 30 mol% all the L16 molecules in the mixed monolayer are electroreducible; moreover, the resulting hydrazocrown ether is reoxidized in a few tens of milliseconds. Over the L16 concentration range from 30 to 90 mol% the average molecular area in the mixed L16–DOPC monolayer at the air | water interface shows a negative deviation from ideal behavior, thus pointing to some kind of aggregation between L16 and DOPC molecules. Over this L16 concentration range, not all the L16 molecules present in the mixed monolayer supported on mercury are electroactive, thus indicating that such an aggregation blocks the L16 molecules in a configuration unfavorable for electron transfer.

Acknowledgements

The authors thank Professor Jan F. Biernat for the samples of the amphiphilic azocrown ether. This work was supported by NATO grant No. 970527 and a grant from The Polish Committee for Scientific Research No. 120-501/66-GR-1268.

References

[1] K.B. Blodgett, J. Am. Chem. Soc. 10 (1935) 1007.
[2] K.B. Blodgett, I. Langmuir, Phys. Rev. 51 (1937) 964.
[3] D. Bizzotto, A. McAlees, J. Lipkowski, R. McCrindle, Langmuir 11 (1995) 3243.
[4] R. Bilewicz, M. Majda, Langmuir 7 (1991) 2794.
[5] J.I. Millán, M. Sánchez-Maestre, L. Camacho, J.J. Ruiz, R. Rodríguez-Amaro, Langmuir 13 (1997) 3860.
[6] C.E. Chidsey, C.R. Bertozzi, T.M. Putvinski, A.M. Mujsce, J. Am. Chem. Soc. 112 (1990) 4301.
[7] S. Sek, A. Misicka, R. Bilewicz, J. Phys. Chem. B 104 (2000) 5399.
[8] M.R. Moncelli, R. Herrero, L. Becucci, R. Guidelli, Israel J. Chem. 37 (1997) 247.
[9] R. Herrero, M.R. Moncelli, L. Becucci, R. Guidelli, J. Phys. Chem. B 101 (1997) 2815.
[10] L.K. Tamm, H.M. McConnel, Biophys. J. 47 (1985) 105.
[11] A. Angelova, R. Ionov, Langmuir 15 (1999) 7199.
[12] I. Prieto, M.T. Martin Romero, L. Camacho, D. Mobius, Langmuir 14 (1998) 4175.
[13] J-Ch. Garringes, I. Rico-Lattes, E. Perez, A. Lattes, Langmuir 14 (1998) 5986.
[14] A. Nelson, A. Benton, J. Electroanal. Chem. 202 (1986) 253.
[15] R. Herrero, F. Tadini Buonisegni, L. Becucci, M.R. Moncelli, J. Electroanal. Chem. 445 (1998) 71.
[16] M.R. Moncelli, L. Becucci, A. Nelson, R. Guidelli, Biophys. J. 70 (1996) 2716.
[17] M.R. Moncelli, R. Herrero, L. Becucci, R. Guidelli, Biochim. Biophys. Acta 1364 (1998) 373.
[18] J.M. Laval, M. Majda, Thin Solid Films 244 (1994) 836.
[19] C.J. Brown, Acta Crystallogr. 21 (1966) 146.
[20] E. Fisher, J. Am. Chem. Soc. 82 (1960) 3249.
[21] E. Laviron, Y. Mugnier, J. Electroanal. Chem. 111 (1980) 337.
[22] M. Shiga, M. Takagi, K. Ueno, Chem. Lett. 1021 (1980).
[23] M. Shiga, H. Nakamura, M. Tahagi, K. Ueno, Bull. Chem. Soc. Jpn. 57 (1984) 412.
[24] J.F. Biernat, E. Luboch, A. Cygan, Y.A. Simonov, A.A. Dvorkin, E. Muszalska, R. Bilewicz, Tetrahedron 48 (1992) 4399.
[25] J.F. Biernat, E. Luboch, A. Cygan, Yu.A. Simon, A.A. Dvorkin, J. Inclusion Phenom. 16 (1993) 209.
[26] E. Muszalska, R. Bilewicz, Analyst 119 (1994) 1235.
[27] H. Huesmann, J. Maack, D. Mobius, J.F. Biernat, Sens. Actuators, B 29 (1995) 148.
[28] L.M. Goldenberg, J.F. Biernat, M.C. Petty, Langmuir 14 (1998) 1236.
[29] I. Zawisza, R. Bilewicz, E. Luboch, J.F. Biernat, J. Electroanal. Chem. 471 (1999) 156.
[30] I. Zawisza, R. Bilewicz, E. Luboch, J.F. Biernat, J. Chem. Soc., Dalton Trans. 4 (2000) 499.
[31] R. Taharo, T. Morozumi, H. Nakamura, M. Shimimura, J. Phys. Chem. B 101 (1997) 7736.
[32] G. Gordillo, D. Schiffrin, J. Chem. Soc., Faraday Trans. 90 (1994) 1913.
[33] M.R. Moncelli, L. Becucci, J. Electroanal. Chem. 385 (1995) 183.
[34] N.S. Matinyan, I.A. Ershler, I.G. Abidor, Biol. Membr. 1 (1985) 451 (in Russian).
[35] M. Carlà, M. Sastre de Vicente, M.R. Moncelli, M.L. Foresti, R. Guidelli, J. Electroanal. Chem. 246 (1988) 283.
[36] J. Ruiz, M.L. Foresti, J. Chem. Soc., Faraday Trans. 1 84 (1988) 4299.
[37] W-Y. Lee, M. Majda, G. Brezesinski, M. Wittek, D. Mobius, J. Phys. Chem. B 103 (1999) 6950.
[38] A.J. Bard, Encyclopedia of Electrochemistry of the Elements, vol. 13, Marcel Dekker, New York, 1974, p. 174.
[39] R. Guidelli, M.L. Foresti, M. Innocenti, J. Phys. Chem. 100 (1996) 18491.
[40] M. Innocenti, M.L. Foresti, A. Fernandez, F. Forni, R. Guidelli, J. Phys. Chem. B 102 (1998) 9667.
[41] C. Buess-Herman, in: J. Lipkowski, P.N. Ross (Eds.), Adsorption of Molecules at Metal Electrodes, WCH, New York, 1992, pp. 77–118.

[42] L. Pohlmann, C. Donner, H. Baumgärtel, J. Phys. Chem. B 101 (1997) 10198.
[43] E. Bosco, S.K. Rangarajan, J. Electroanal. Chem. 129 (1981) 25.
[44] E. Bosco, S.K. Rangarajan, J. Chem. Soc., Faraday Trans. 1 77 (1981) 483 (see also p. 1673).
[45] M. Noel, S. Chandrasekaran, C.A. Basha, J. Electroanal. Chem. 222 (1987) 93.
[46] B. Bhattacharjee, S.K. Rangarajan, J. Electroanal. Chem. 302 (1991) 207.
[47] M.H. Hölzle, U. Retter, D.M. Kolb, J. Electroanal. Chem. 371 (1994) 101.
[48] D.C. Pestana, P.P. Power, Inorg. Chem. 30 (1991) 528.
[49] D. Bizzotto, E. Wong, Y. Yang, J. Electroanal. Chem. 480 (2000) 233.
[50] R.A. Hann, in: G.G. Roberts (Ed.), Langmuir–Blodgett films, Plenum Press, New York, 1990, p. 17 (Ch. 2).
[51] A. Nelson, N. Aufret, J. Electroanal. Chem. 244 (1988) 99.
[52] A. Nelson, N. Aufret, J. Electroanal. Chem. 248 (1988) 167.